The Contribution of Ionizing Stars to theFar-Infrared and Radio Emission in the Milky Way: Evidence for a Swept-up Shell and Diffuse Ionized Halo around the W4 Chimney/Supershell

S. Terebey[1], M. Fich[2], R. Taylor[3], Y. Cao[4]

[1]Extrasolar Research Corporation, 569 S. Marengo Ave., Pasadena, CA 91101

[2]Dept. of Physics and Astronomy, University of Waterloo, Waterloo, CA

[3]Dept. of Physics and Astronomy, University of Calgary, Calgary, CA

[4]KLA Tencor Corp., San Jose, CA

Received _____; accepted _____

ABSTRACT

Normandeau et al. (1996) have proposed that W4 is a galactic chimney, the only chimney to-date identified in our Galaxy. Using the recent $\sim 1'$ resolution IGA and DRAO CGPS galactic plane surveys we analyze the far-infrared and radio structure of the W4 chimney/supershell. We show W4 has a swept-up partially ionized shell of gas and dust which is powered by the OCl 352 star cluster. Analysis of the dust column density establishes there is dense interstellar material below the shell, directly showing the dense material which caused the lower shell expansion to stall. Due to much lower densities above the Galactic plane, the upper W4 shell achieved "breakout" to form a Galactic chimney. Although the shell appears ionization bounded, it is very inhomogenous and an ionized halo provides evidence of significant Lyman continuum leakage. A large fraction of the OCl 352 cluster photons escape to large distances and are available to ionize the WIM (warm ionized medium) component of the interstellar medium.

Subject headings: Galaxy:structure — HII regions — infrared: ISM: continuum — ISM:bubbles — ISM:individual(W4 Supershell) — ISM: structure — radio continuum: ISM

1. Introduction

The *IRAS* Galaxy Atlas (IGA) provides high spatial resolution processed *IRAS* images of the Galactic plane at far-infrared wavelengths (Cao et al. 1997). The IGA, in conjunction with the DRAO HI line/21 cm continuum (Normandeau et al. 1997) and FCRAO CO(1-0) line (Heyer et al. 1998) Galactic plane surveys, both with similar ($\sim 1'$) resolution, provide a powerful venue for studying the interstellar medium and large scale

structure in our Galaxy.

Figure 1 shows a panoramic view encompassing the W3, W4, and W5 HII regions (Westerhout 1958) in the Outer Galaxy. In the infrared W4 and W5 display pronounced loop structure, suggestive of wind-swept shells powered by OB clusters, while W3's compact size indicates a young HII region which is related to star formation activity in the W3 molecular cloud. Comparison of the 60 μmemission (left panel) with the 21 cm continuum emission (right panel) illustrates the close correspondence of the far-infrared to radio continuum emission. Previous studies show the ratio of far-infrared to 2.7 GHz radio continuum flux density R is high for HII regions ($\sim$ 1000) as compared with supernova remnants ($<$ 10) (Furst et al. 1987; Haslam & Osborne 1987). Based on this discriminator between thermal and nonthermal regions, most of the structure in Figure 1 is likely due to thermal emission.

The W4 HII region provides a striking example of dynamically formed features in the ISM. Normandeau, Taylor, and Dewdney (1996) propose W4 is a superbubble powered by the OCl 352 (IC1805) OB cluster (l = *135* deg, b = *1* deg) which has achieved breakout to form a Galactic chimney. The evidence for a chimney includes a large void in the HI gas above the IC1805 cluster (Normandeau et al. 1996) (indicated schematically in Fig. 1), as well as an accompanying Hα shell (Dennison et al. 1997). Directly below OCl 352 and prominent in Figure 1 is the smaller W4 loop ($\sim$ 40′), visible in infrared, radio continuum and Hα emission. The W4 loop is interpreted as the lower half of the W4 superbubble, which is smaller in size below OCl 352 because it has expanded into a higher ambient density medium. Basu, Johnstone, & Martin (1999) model the W4 region as wind-blown bubble in a stratified interstellar medium.

The correspondence in Figure 1 between the 60 μmemission (left panel) and 21 cm continuum emission (right panel) is very strong. Notable is the large 100 pc loop of ionized

material which is mirrored in the 60 μmdata in the 1.8° × 2.5° field. Marked near the top is the OCl 352 OB cluster, the ionization source for the HII region. The ratio of the 60μm/100μm data (not shown) displays a gradient which locates the hottest dust near OCl 352, decreasing to cooler dust temperatures in the loop.

The stellar properties and distance to the OCl 352 cluster have been measured by Massey, Johnson, & DeGioia-Eastwood (1995). A trio of massive stars (O4-O5) provide most of the ionizing radiation. The FIR and radio emission are not symmetric around the cluster: to the north (outside the boundaries of Fig. 2; but see Fig. 1) lies little emission except for a dense cometary-shaped cloud which is being photoionized and eroded by the OB cluster (Heyer et al. 1996b). This suggests much lower densities on average, north of the cluster, compared with the southern region shown in Figure 2.

There is a halo of faint ionized gas around W4. The correspondence of 60 μm and 21 cm continuum continues to much lower intensities than can be seen in the stretch provided in Figure 2. The data indicate there is extensive faint ionized gas centered on the HII region, but lying well outside the W4 loop.

The picture supports the view that the OB cluster in a central role. Strong winds from the cluster are probably responsible for sweeping up the 100 pc sized loop (or shell) of material.

2. Data and Analysis

3. The Structure of the W4 Loop

3.1. Radio versus Infrared Comparison

Figure 2 demonstrates there is a strong correspondance between the 60 μmand 21 cm continuum images. The correspondance is not automatic, as the far-infrared emission is sensitive to warm (20 - 60 K) dust, whereas the 21 cm continuum traces ionized (> 3000 K) gas. There is an overall correlation with slope R = $I_{21cm}/I_{60\mu m} \sim 300$ with significant scatter. To understand the source of the "scatter", we map the outlying points points back into image space, to look for geometrically distinct regions. We adopt the excess map technique of Gaustad & Van Buren (1993) and form a difference image, $I_{21cm} - R \times I_{60\mu m}$, which serves to eliminate structure common to both images.

The remarkable difference image (Fig. 2, middle panel) reveals striking spatial differences between ionized gas and warm dust. The loop structure displays enhanced 21 cm emission (white) lying interior to the enhanced 60μmemission (black). The IC1805 star cluster is the likely source of ionization; crosses mark the positions of the three earliest type (O4-O5) massive stars. The enhanced continuum emission on the inner edge suggests the loop is ionization bounded.

The far-infrared emission is generally accepted to be thermal emission from dust heated by the UV component of the local interstellar radiation field (Terebey & Fich 1986). On this basis, the enhanced FIR at the outer loop edge appears due to non-ionizing UV photons from the OB cluster which travel into the compressed shell where the dust optical depth is significant. The infrared data (see section 3.2 show a corroborating gradient in the dust temperature across the shell.

The faint halo of ionized gas outside the W4 loop, seen primarily to the left and top, is not consistent with an ionization bounded HII region. This further suggests the wind-blown shell is patchy rather than homogeneous. If the shell is patchy, i.e. the ionization is density bounded at some but not all points, then ionizing photons can leak through and potentially ionize the low-density ICM out to quite large distances.

3.2. Dust temperature and optical depth from infared data

We express the dust opacity as $\kappa = (0.1 cm^2 g^{-1} (250 \mu m / \lambda_{\mu m})^{\beta}$ (Hildebrand 1983) where $\lambda_{\mu m}$ is the wavelength in microns and $\beta = 0$ - 2 is a standard range; we adopt $\beta = 1$ for far-infrared wavelengths. The dust optical depth $\tau = \kappa \rho$ where ρ is the gas density. The intensity due to thermal dust emission is then, for optically thin emission, $I = \kappa \rho B_{\nu}(T_D)$ where B_{ν} is the Planck function and T_D is the dust temperature. The dust temperature is derived from the 60 and 100 μmintensity ratio, where the 60 μm data is beam-matched to the 100 μmresolution. The background emission from cold ($\sim$ 20 K) cirrus emission associated with HI clouds is subtracted from both the 60 and 100 μmimages. The background model multiples the integrated HI brightness temperature image by an HI-to-FIR conversion constant. The adopted conversion constant was derived by Terebey & Fich (1986) for the infrared cirrus in a nearby ($l = 125$ °) field. The background model has little spatial structure and is constant to within 10% over the field of interest, having a value 10.6 $\pm$ 1.0 MJy ster^{-1} at 60 μm). The IRAS intensity ratio is then color-corrected (*IRAS* Catalogs and Atlases: Explanatory Supplement 1988); for example changing the median 60 to 100 intensity ratio in the loop from 0.52 to XX for $\beta = 1$ dust opacity.

3.3. Shell Model versus Ring Model

Two physical models are suggested by the loop morphology of W4: a thin limb-brightened shell, or a physical ring, i.e. torus of material. The ring model predicts no material projected toward the geometric center. The thin shell model with thickness T has a path length 2T toward the geometric center and a contrast between center and limb-brightened edge depends on shell thickness.

The spatial structure in the optical depth map implies there are large density variations across the W4 loop. Nevertheless the loop structure is sufficiently regular to attempt fitting a shell model. The spherical assumption is admittedly simplistic, as the IC1805 powering star cluster lies at the top edge, rather than geometric center of the model. Figure 3 and 4 display two models which give reasonable visual fits. Figure 3 displays the optical depth data in green whereas Model 1 is overlaid in red. Three slices through the data are displayed in Figure 4. Two models are overlaid; the shell thickness in model 2 is one quarter that of model 1, and exhibits correspondingly stronger limb-brightening. Model parameters are given in Table 1.

4. Discussion

We have shown there is a strong correspondence between the FIR and radio continuum in the *IRAS* IGA and DRAO 21 cm Galactic plane surveys (Fig. 1). The emission is due to thermal processes (dust and ionized gas). Analysis of a subregion centered on the lower W4 loop supports the Normandeau et al. (1996) W4 chimney hypothesis where a swept-up shell is powered by the OCl 352 OB cluster. Fits to the far-infrared data reveal the shell. If most of the shell is neutral, then the derived shell mass is about 10,000 $M_\odot$ with density 4.8 cm^{-3}, implying about 2.8 cm^{-3} for the ambient density. The ionized gas

appears interior to the dust, suggesting the shell is ionization bounded. However the shell is very inhomogenous, varying by at least factors of three in density. A halo of ionized gas and heated dust is seen outside the shell on left side. This is direct evidence of Lyman continuum photon leakage. Analysis of the emission measure shows that even though the shell is ionization bounded in some areas, that most of the ionizing photons escape the shell. This supports recent proposals that O stars provide the ionizing photons which are needed to produce the extended WIM which is observed in external galaxies (Ferguson et al. 1996; Oey & Kennicutt 1997).

REFERENCES

Basu, S., Johnstone, D., & Martin, P. G. 1999, ApJ, 515, 843

Boulanger, F., Beichman, C. A., Desert, F. X., Helou, G., Perault, M., & Ryter, C. 1988, ApJ, 332, 328

Cao, Y., Terebey, S., Prince, T. A., & Beichman, C. A. 1997, ApJS, 111, 387

Dennison, B., Topasna, G. A., & Simonetti, J. H. 1997, ApJ, 474, L31

Fowler, J. 1994, in "Science with High-Spatial Resolution Far-Infrared Data", eds. S. Terebey & J. Mazzarella, (Pasadena: JPL), p. 1

Furst, E., Reich, W., & Sofue, Y. 1987, A&AS, 71, 63

Gaustad, J. E. & Van Buren, D. 1993, PASP, 105, 692

Haslam, C. G. T. & Osborne, L. L. 1987, Nature, 327, 211

Heyer, M. H., Brunt, C., Snell, R. L., Howe, J., Schloerb, F. P., & Carpenter, J. H.. 1998, ApJS, 115, 241

Heyer, M. H. & Terebey, S. 1998, ApJ, 502, 265

Hildebrand, R. H. 1983, Quart. J. R. A. S., 24, 267

IRAS Catalogs and Atlases: Explanatory Supplement 1988, ed. C. A. Beichman, Neugebauer, G., Habing, H. J., Clegg, P. E., & Chester, T. J., (Washington, DC: GPO)

Normandeau, M., Taylor, A. R., & Dewdney, P. E. 1996, Nature, 380, 687

Normandeau, M., Taylor, A. R., & Dewdney, P. E. 1997, ApJL, 108, 279

Terebey, S. & Fich, M. 1986, ApJ, 309, L73

This manuscript was prepared with the AAS LaTeX macros v5.0.

Table 1. Parameters of W4 Dust Shell Model[a].

Model	$l_{cen}(°)$	$b_{cen}(°)$	δR(′)	$R_{in}(')$	R_{in}(pc)	τ_{cen}	$n_H(cm^{-3})$	$M_{sh}(M\odot)$
I	135.02	0.42	10	30	19	0.00011	4.8	6700
II	135.02	0.42	2.5	30	19	0.00011	19	5300

[a]Assumes D = 2.2 kpc, κ =0.25 cm^2 g^{-1} at 100 μm, mean mass per H = 1.4

Table 2. Parameters of W4 Ionized Shell Model[a].

Model	$l_{cen}(°)$	$b_{cen}(°)$	δR(′)	$R_{in}(')$	R_{in}(pc)	$n_e^2 L$(pc cm^{-6})	$n_e(cm^{-3})$	$M_{sh}(M\odot)$
I	135.02	0.42	10	30	19	270	3.3	4800
II	135.02	0.42	2.5	30	19	270	13	2600

[a]Size and thickness of model shell is the same as Table 1.

Fig. 1.— Panoramic far-infrared and radio images of the W3-4-5 Outer Galaxy HII regions. The strong correspondence between the infrared and radio continuum emission toward the HII regions demonstrates a tight coupling between warm dust (60 and 100 μm) and ionized gas (21 cm). Inverse color table used, so bright = black. Left panel shows *IRAS* 60 μm data; 100 μm looks nearly identical. Notice both W4 and W5 exhibit loop structure, suggestive of limb-brightened shells. Display uses $1.0 < \log I_{60}(\mathrm{MJy\ ster^{-1}}) < 2.5$. Right panel shows 21 cm continuum emission; 72 cm continuum looks nearly identical. The W3, W4, and W5 HII regions and HB3 supernova remnant are identified. W3 is a region of active star formation. Solid line shows the approximate outline of the proposed W4 Galactic chimney; this model invokes a density gradient to explain breakout to the top (Normandeau et al. 1996). Display uses $0 < \log I_{21}(\mathrm{K}) < 1.2$, in brightness temperature units.

Fig. 2.— A closeup of the W4 loop region shows striking spatial differences between the infrared and radio continuum emission. Difference images shows ionized gas (white) lies interior to warm dust (black) across the shell. Positions of the three earliest O stars in the IC1805 OB cluster are marked. Default color table used, so bright = white. Left panel shows 60 μm data. Display uses $0.5 < \log I_{60}(\mathrm{Jy\ arcmin^{-2}}) < 2.5$. Right panel shows 21 cm continuum data, $-2.1 < \log I_{21}(\mathrm{Jy\ arcmin^{-2}}) < -1.2$. Middle panel shows difference image, as described in text. Display uses $-0.02 > I_{diff} < 0.015$.

Fig. 3.— The optical depth and temperature across the W4 loop. Left panel shows background subtracted 60 μm image. As the other panels demonstrate, most of the structure represents column density rather than temperature variation. The IC1805 OB cluster is the likely source of ionization and heating. Display uses $0.5 < \log I_{60}(\mathrm{MJy\ ster^{-1}}) < 2.5$. The τ_{100} optical depth map (middle panel) reveals dense relatively cool material below ($b < 0°$) the limb-brightened shell. This dense material is predicted by the W4 chimney model, to explain why breakout occurs above rather than below the powering IC1805 cluster. The

shell is inhomogenous; low column density extends from the lower-middle (135.0, 0.2) to the left. Display uses -5.0 < log τ_{100} < -3.0. Low intensity regions (I_{60} < 0.5 MJy ster^{-1}) are masked out to minimize unreliable structure due to noise (middle and right panel)(???check value). Right panel shows dust color temperature derived from the I_{60}/I_{100} intensity ratio. Overplotted are τ_{100} = 0.0002 (thin), 0.0005 (thick) optical depth contours. The dust temperature is nearly constant at 36 K, roughly centered on IC1805; to the left the warm dust extends far past the barely-visible shell edge. The shell is much thicker to the lower right; there is a corresponding abrupt temperature decrease at the shell's inner edge. Display uses 25 < T_c(K) < 45.

Fig. 4.— a) The W4 thick-shell model (red) is superimposed on the optical depth map (green) of the dust at 100 microns. The numbered lines indicate the positions of plotted slices, which show optical depth versus distance from the nominal shell center. b) The data (solid-line) and two models from Table 1 are shown. Models have been convolved with the 100 μm beam. Deviations from sphericity favor the thick-shell model, while the sharp horns of the line profiles favor the thin-shell model. The shell is patchy, but appears consistent with an inhomogenous shell rather than a thin ring, i.e. torus.

Fig. 5.— a) The W4 thin-shell model (red) is superimposed on the 21 cm radio image (green) of the ionized gas. The numbered lines indicate the positions of plotted slices. b) The profiles of observed and predicted radio emission versus distance from the nominal shell center. The data (solid-line) and two models from Table 2 are shown. Models have been convolved with the 21 cm beam. The sharp horns of the line profiles favor the thin-shell model. The ionized shell is patchy, but appears consistent with a shell rather than a thin ring, i.e. torus. Figure 2 shows that the ionized gas lies interior to the dust emission, suggesting the shell is ionization bounded.

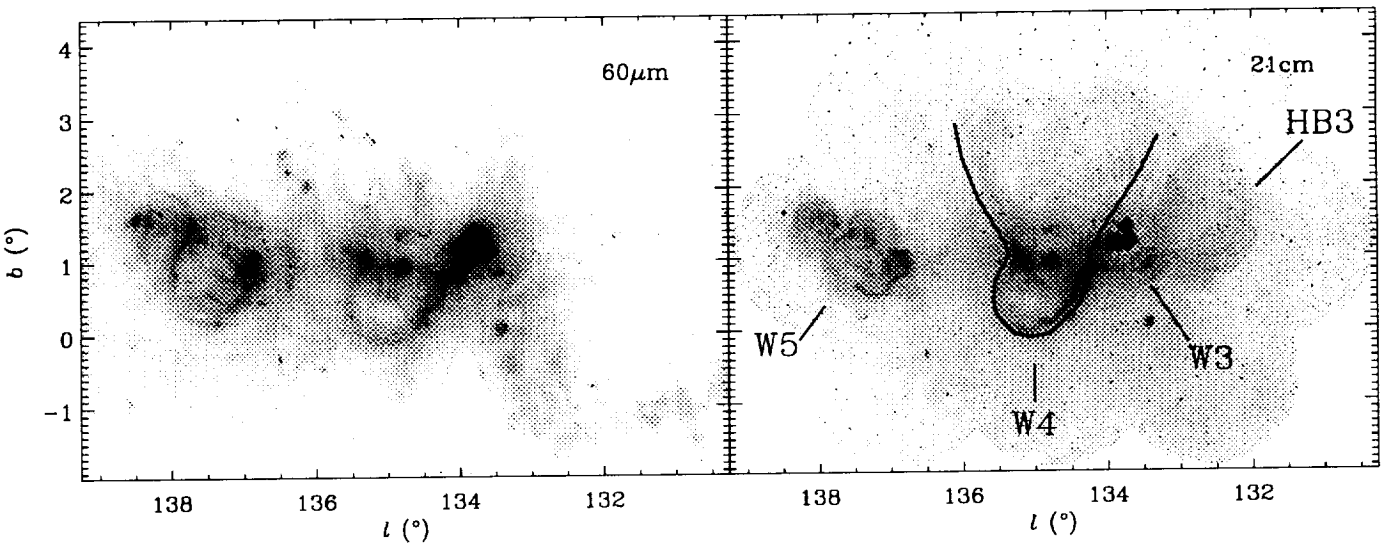
60μm
21cm
HB3
W5
W4
W3
b (°)
l (°)
l (°)
4
3
2
1
0
−1
138
136
134
132
138
136
134
132

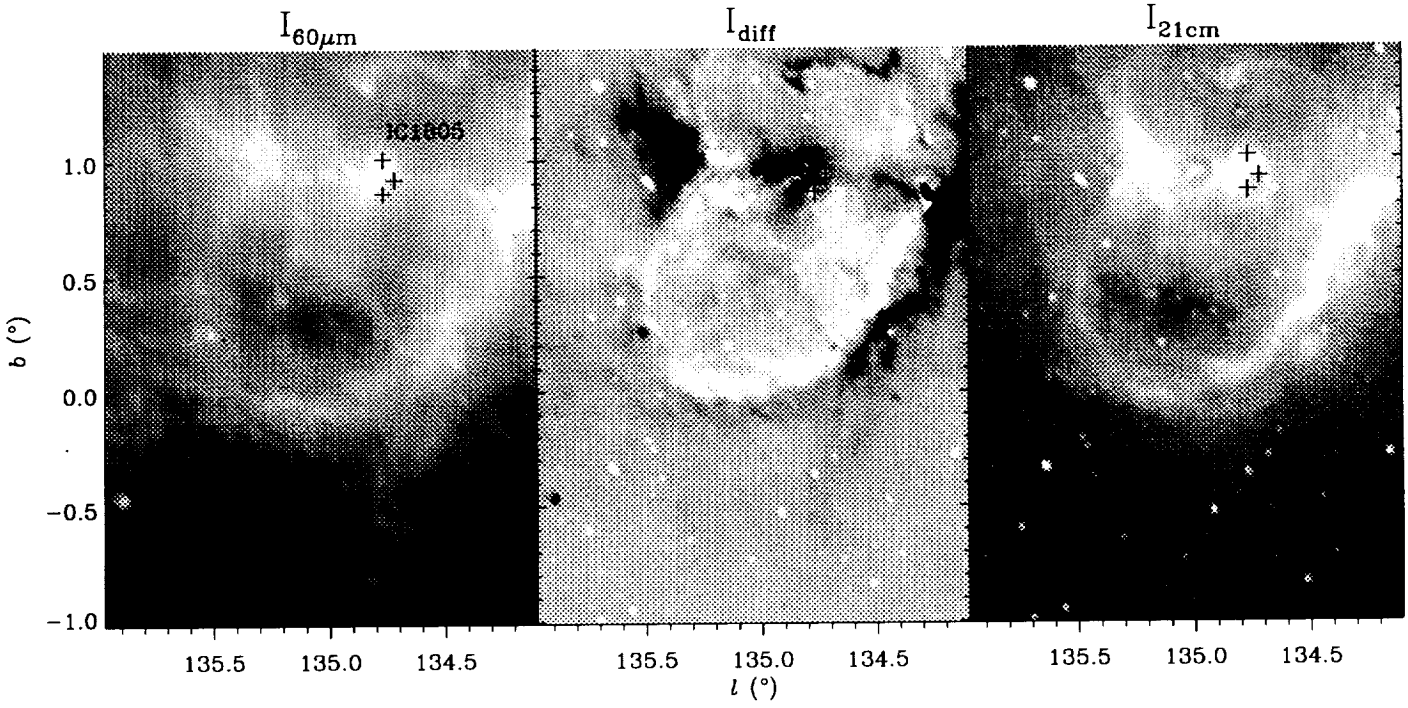
$I_{60\mu m}$
I_{diff}
I_{21cm}
IC1805
1.0
0.5
0.0
−0.5
−1.0
b (°)
135.5
135.0
134.5
135.5
135.0
134.5
135.5
135.0
134.5
l (°)

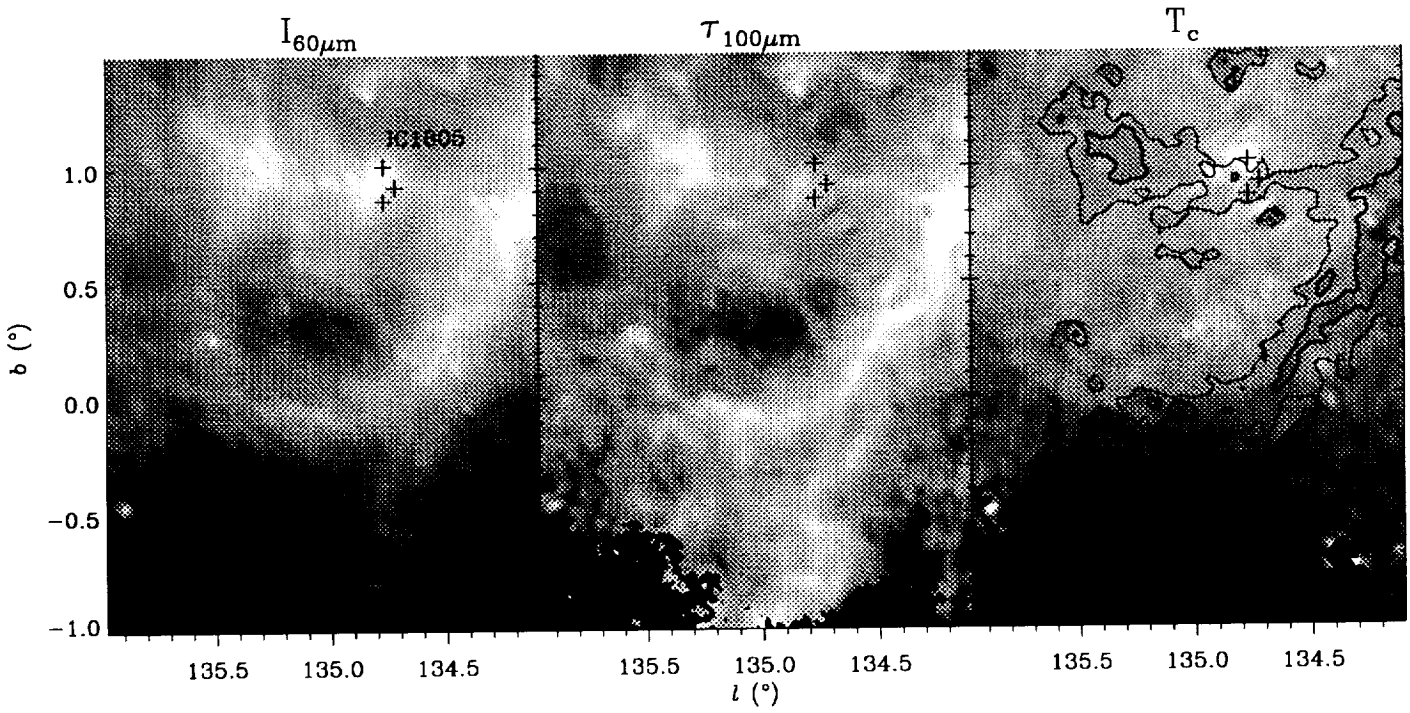
$I_{60\mu m}$
$\tau_{100\mu m}$
T_c
IC1805
1.0
0.5
0.0
−0.5
−1.0
b (°)
135.5
135.0
134.5
135.5
135.0
134.5
135.5
135.0
134.5
l (°)

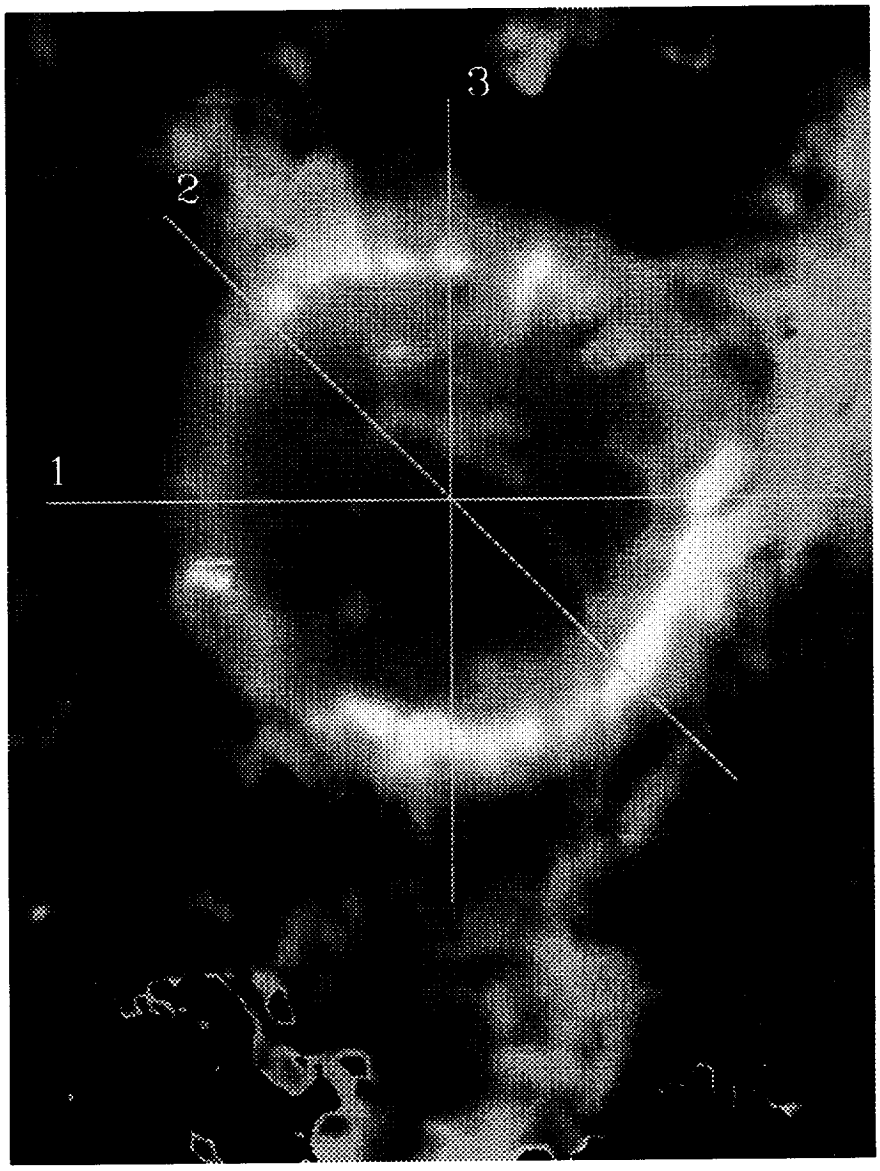
3
2
1

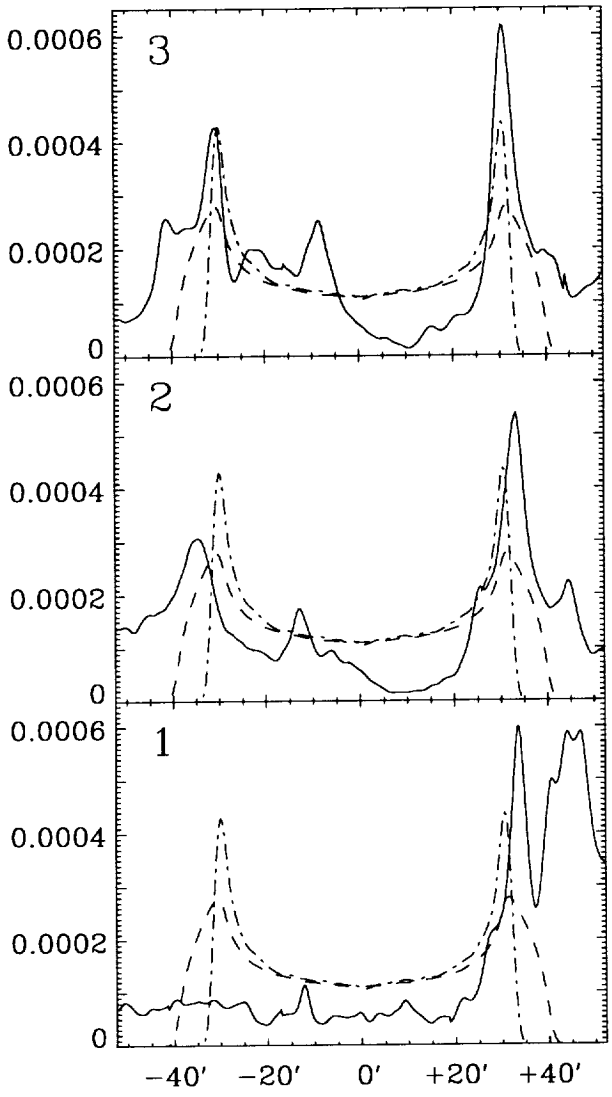
0.0006
0.0004
0.0002
0
3
0.0006
0.0004
0.0002
0
2
0.0006
0.0004
0.0002
0
1
−40′
−20′
0′
+20′
+40′

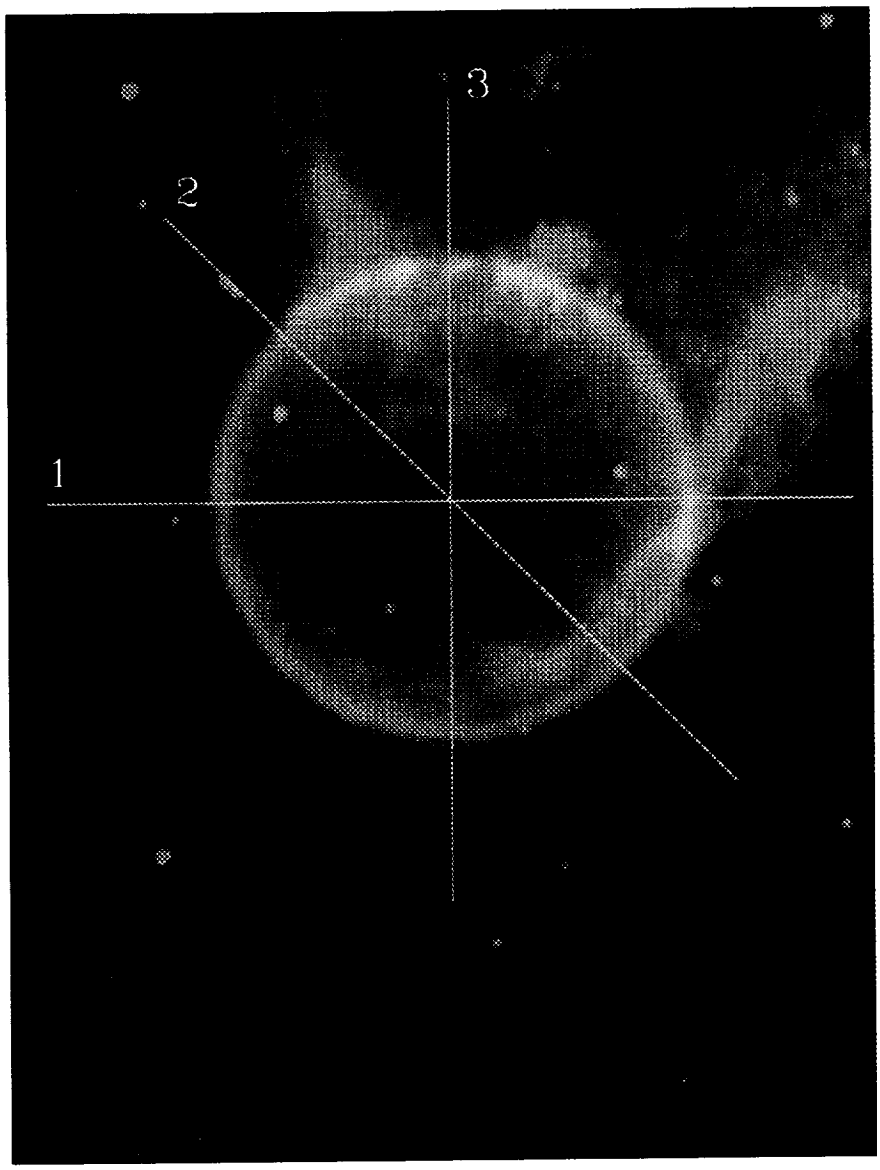
3
2
1

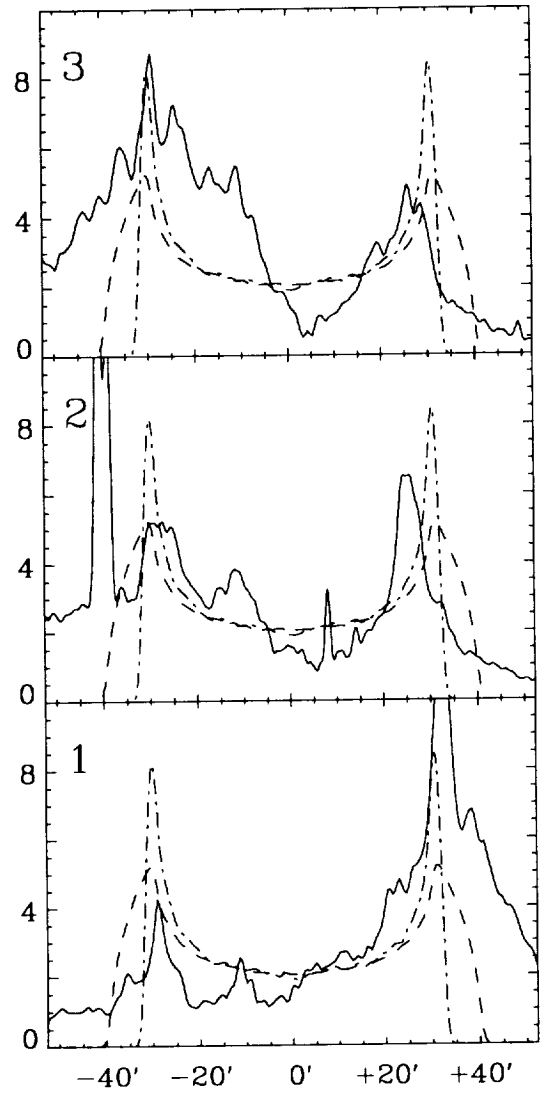
3
2
1
8
4
0
−40′
−20′
0′
+20′
+40′

National Aeronautics and Space Administration

Report Documentation Page

1. Report No.	2. Government Accession No.	3. Recipient's Catalog No.

4. Title and Subtitle
The Contribution of Ionizing Stars to the Far-Infrared and Radio Emission in the Galaxy

5. Report Date
12/18/99

6. Performing Organization Code

7. Author(s)
Dr. Susan Terebey

8. Performing Organization Report No.

10. Work Unit No.

9. Performing Organization Name and Address
Extrasolar Research Corporation
720 Magnolia Ave., Pasadena CA 91106

11. Contract or Grant No.
NAS5-97066

13. Type of Report and Period Covered
Final Rpt 1/97-12/99

12. Sponsoring Agency Name and Address
NASA Goddard Space Flight Center
Space Science Procurement Office, Code 216
Green Belt MD 20771

14. Sponsoring Agency Code

15. Supplementary Notes

16. Abstract

S. Terebey summarizes research activities carried out in this eigth and final progress report. The final report includes: a summary document, copies of three published research papers, plus a draft manuscript of a fourth research paper entitled "The Contribution of Ionizing Stars to the Far-Infrared and Radio Emission in our Galaxy: Evidence for a Swept-up Shell and Diffuse Ionized Halo Around the W4 Chimney/Supershell," by authors S. Terebey, M. Fich, R. Taylor, and Y. Cao. We show W4 has a swept-up partially ionized shell of gas and dust which is powered by the OCl 352 star cluster. Analysis shows there is dense interstellar material directly below the shell, evidence that the lower W4 shell "ran into a brick wall" and stalled, whereas the upper W4 shell achieved "breakout" to form a Galactic chimney. An ionized halo is evidence of Lyman continuum leakage which ionizes the WIM (warm ionized medium).

17. Key Words (Suggested by Author(s))	18. Distribution Statement		
	Unclassified- Unlimited		
19. Security Classif. (of this report)	**20. Security Classif. (of this page)**	**21. No. of pages**	**22. Price**
Unclassified	Unclassified	67	

NASA FORM 1626 OCT 86